J|A|C|S
ARTICLES
Published on Web 09/06/2006

Arsenic Binding to Human Metallothionein

Thanh T. Ngu and Martin J. Stillman*

Contribution from the Department of Chemistry, The University of Western Ontario, London, Ontario, Canada, N6A 5B7

Received April 26, 2006; E-mail: Martin.Stillman@uwo.ca

Abstract: The number of reported cases of chronic arsenic poisoning is on the rise throughout the world, making the study of the long-term effects of arsenic critical. As^{3+} binds readily to biological thiols, including mammalian metallothionein (MT), which is an ubiquitous sulfur-rich metalloprotein known to coordinate a wide range of metals. The two-domain mammalian protein binds divalent metals (M) into two metal−thiolate clusters with stoichiometries of M_3S_{cys9} (β) and M_4S_{cys11} (α). We report that As^{3+} binds with stoichiometries of As_3S_{cys9} (β) and As_3S_{cys11} (α) to the recombinant human metallothionein (rhMT) isoform 1a protein. Further, we report the complete kinetic analysis of the saturation reactions of the separate α and β domains of rhMT with As^{3+}. Speciation in the metalation reactions was determined using time- and temperature-resolved electrospray ionization mass spectrometry. The binding reaction of As^{3+} to the α and β MT domains is shown to be noncooperative and involves three sequential, bimolecular metalation steps. The analyses allow for the first time the complete simulation of the experimental data for the stepwise metalation reaction of MT showing the relative concentrations of the metal-free, apo MT and each of the As-MT intermediate species as a function of time and temperature. At room temperature (298 K) and pH 3.5, the individual rate constants for the first, second, and third As^{3+} binding to apo-αMT are 5.5, 6.3, and 3.9 M^{-1} s^{-1} and for apo-βMT the constants are 3.6, 2.0, and 0.6 M^{-1} s^{-1}. The activation energy for formation of As_1-H_6-βMT is 32 kJ mol^{-1}, for As_2-H_3-βMT it is 35 kJ mol^{-1}, for As_3-βMT it is 29 kJ mol^{-1}, for As_1-H_8-αMT it is 33 kJ mol^{-1}, for As_2-H_5-αMT it is 29 kJ mol^{-1}, and for As_3-H_2-αMT it is 23 kJ mol^{-1}.

Introduction

International concern over arsenic ingestion from drinking water has increased over the past decade as the number of reported cases of chronic arsenic poisoning has risen dramatically.[1] Chronic arsenic exposure or arsenicism may lead to hyperkeratosis, skin lesions, and cancer of the skin, lung, bladder, and kidney.[2] Worldwide exposure to arsenic is a significant health risk to populations in many countries. In particular, chronic arsenic poisoning in Bangladesh and West Bengal as a result of exposure to drinking water that contains natural arsenic affects a large fraction of the population. While means to purify arsenic-contaminated waters and soil are vitally important, a better understanding of the arsenic metabolic pathway in mammals, and humans in particular, is also essential.

Earthworms from the Lumbricidae family have been found to inhabit arsenic-rich soils[3−6] that contain up to 34 000 mg As kg^{-1} dry soil weight[5,7] and have been suggested as a potential biomarker for metals and metalloids. Further, the earthworm *Lumbricus rubellus* has been reported to contain concentrations up to 1000 mg As kg^{-1}.[4] XAS analysis of *L. rubellus* suggests that 30% of As^{3+} is coordinated with sulfurs, suggesting binding to metallothionein.[8] Sturzenbaum et al.[9,10] have identified and cloned two metallothionein (MT) isoforms from *L. rubellus* that contain 21 cysteines and bind cadmium. It is necessary to understand the rate and stoichiometry of arsenic binding to MT and other arsenic-binding proteins in earthworms before earthworms can be used as biomarkers.

The bioinorganic chemistry of arsenic suggests that a reduction of As^{5+} to As^{3+} occurs through the interaction with thiols and subsequent binding of As^{3+} to the thiols. The reduction is catalyzed by arsenate reductases, which are thought to be the first step in the detoxification of arsenic.[11] The toxic effects of As^{3+} may be the result of reactions with sulfydryl groups that are essential for the mitochondrial oxidation of pyruvate and oxoglutarate.[12] As^{3+} binds strongly to the thiol group in cysteine, making glutathione (GSH)[13−19] and MT[20−22] prime targets. Although As^{3+} binding to MT has been reported for the metal-

(1) Mead, M. N. *Environ. Health Perspect.* **2005**, *113*, A378−A386 and other articles within this issue.
(2) Hughes, M. F. *Toxicol. Lett.* **2002**, *133*, 1−16.
(3) Geiszinger, A.; Goessler, W.; Kuehnelt, D.; Francesconi, K. A.; Kosmus, W. *Environ. Sci. Technol.* **1998**, *32*, 2238−2243.
(4) Langdon, C. J.; Piearce, T. G.; Black, S.; Semple, K. T. *Soil Biol. Biochem.* **1999**, *31*, 1963−1967.
(5) Langdon, C. J.; Piearce, T. G.; Meharg, A. A.; Semple, K. T. *Soil Biol. Biochem.* **2001**, *33*, 1239−1244.
(6) Morgan, A. J.; Winters, C.; Yarwood, A. *Cell Biol. Int.* **1994**, *18*, 911−914.
(7) Goodridge, J. C. *Reports of the Devonshire Association* **1964**, *96*, 228−267.
(8) Langdon, C. J.; Meharg, A. A.; Feldmann, J.; Balgar, T.; Charnock, J. M.; Farquhar, M.; Piearce, T. G.; Semple, K. T.; Cotter-Howells, J. *J. Environ. Monit.* **2002**, *4*, 603−608.
(9) Sturzenbaum, S. R.; Kille, P.; Morgan, A. J. *FEBS Lett.* **1998**, *431*, 437−442.
(10) Sturzenbaum, S. R.; Winters, C.; Galay, M.; Morgan, A. J.; Kille, P. *J. Biol. Chem.* **2001**, *276*, 34013−34018.
(11) Demel, S.; Shi, J.; Martin, P.; Rosen, B. P.; Edwards, B. F. P. *Protein Sci.* **2004**, *13*, 2330−2340.
(12) Johnstone, R. M. In *Metabolic Inhibitors: Comprehensive Treatise*, 2nd ed.; Hochster, R. M., Quastel, J. H., Eds.; Academic Press: New York, 1963; pp 99−118.

free or apo human MT isoform 2,[22] rabbit,[20] and the seaweed *Fucus vesiculous* protein,[21] no mechanistic details have previously been described.

Metallothionein is a thiol-rich (approximately 30% of its amino acid sequence), low molecular weight (approximately 6000 Da), metal-binding protein that is ubiquitous in nature but particularly abundant in the liver and kidneys of mammals.[23−26] Metallothionein biosynthesis can be induced by steroids, hormones, cytotoxic agents,[27] and a wide range of metals,[23−26] including As^{3+}.[28] MT has also been shown to bind a range of metals in vivo and in vitro, including Bi^{3+}, Cu^{+}, Ag^{+}, Au^{+}, Hg^{2+}, Cd^{2+}, Zn^{2+},[23−26] and As^{3+}.[20−26] Previous studies have shown that MT 1 and 2 isoforms may play a protective role in chronic inorganic arsenic poisoning in mice.[29]

Figure 1 shows the sequence of the human α and β domains and the recombinant S-tag. Figure 2 shows the molecular model of mammalian MT and the α and β metal−sulfur clusters.

Kinetic studies carried out on MT thus far have either used metalated MT and a ligand that displaces the metal through blockage of the cysteinyl thiols, by competitive metal transfer, or metalated the Zn-containing protein directly with a second metal that exhibits a greater binding constant (e.g., Cu^{+}). Competitive ligands previously studied included EDTA[31,32] and nitrilotriacetate[33] for metal transfer and *N*-ethylmaleimide[34] and DTNB for thiol blockage.[35] Kinetic studies of the metalation of MT have included *cis*-dichlorodiammineplatinum(II)[36] and the metal ions Cu^{+},[37] Zn^{2+}, Cd^{2+}, and Co^{2+}.[38] However, in most of these studies, the intermediate species present could not be unambiguously identified because the instruments used (stopped-

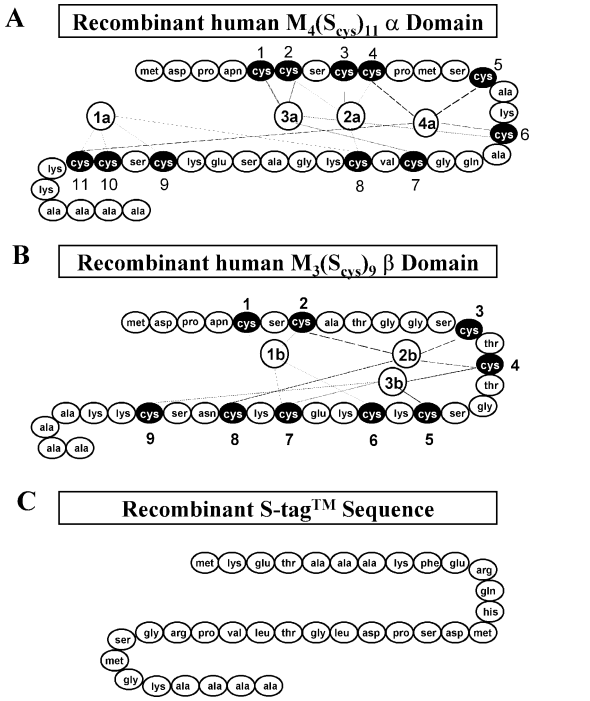

Figure 1. Sequence of (A) the human α domain showing the connectivities for four divalent metal ions (labeled 1a−4a) to 11 cysteines, (B) the human β domain showing the connectivities for three divalent metal ions (labeled 1b−3b) to nine cysteines, and (C) the recombinant S-tag. The numbers on the cysteines are consistent with the numbering scheme shown in Figure 2 and have been used previously[25,30] for the recombinant protein.

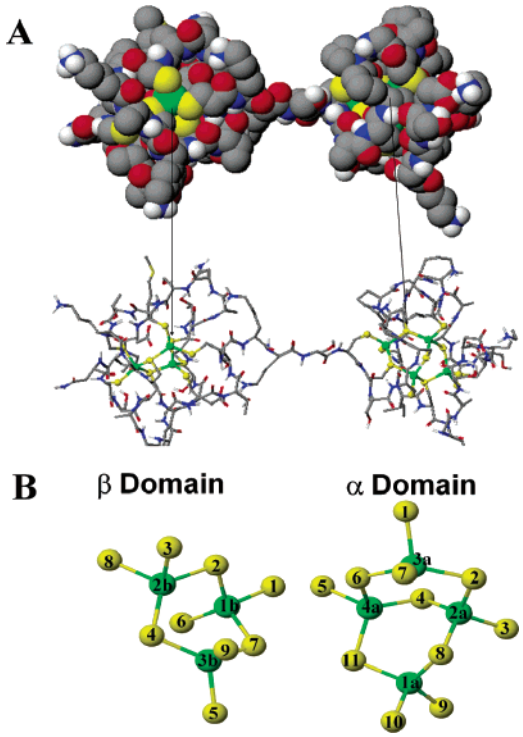

Figure 2. (A) Molecular model of mammalian MT and (B) the α and β metal−sulfur clusters with divalent metals tetrahedrally coordinated to the cysteines. Green atoms correspond to divalent metal cations, and yellow atoms correspond to sulfurs from cysteines. The numbers correspond to the amino acid sequence shown in Figure 1 and have been used previously[25,30] for the recombinant protein.

(13) Manley, S. A.; George, G. N.; Pickering, I. J.; Glass, R. S.; Prenner, E. J.; Yamdagni, R.; Wu, Q.; Gailer, J. *Chem. Res. Toxicol.* **2006**, *19*, 601−607.
(14) Gailer, J.; George, G. N.; Pickering, I. J.; Prince, R. C.; Younis, H. S.; Winzerling, J. J. *Chem. Res. Toxicol.* **2002**, *15*, 1466−1471.
(15) Gailer, J.; George, G. N.; Pickering, I. J.; Prince, R. C.; Ringwald, S. C.; Pemberton, J. E.; Glass, R. S.; Younis, H. S.; DeYoung, D. W.; Aposhian, H. V. *J. Am. Chem. Soc.* **2000**, *122*, 4637−4639.
(16) Raab, A.; Meharg, A. A.; Jaspars, M.; Genney, D. R.; Feldmann, J. *J. Anal. At. Spectrom.* **2004**, *19*, 183−190.
(17) Scott, N.; Hatlelid, K. M.; MacKenzie, N. E.; Carter, D. E. *Chem. Res. Toxicol.* **1993**, *6*, 102−106.
(18) Rey, N. A.; Howarth, O. W.; Pereira-Maia, E. C. *J. Inorg. Biochem.* **2004**, *98*, 1151−1159.
(19) Serves, S. V.; Charalambidis, Y. C.; Sotiropoulos, D. N.; Ioannou, P. V. *Phoshorus, Sulfur Silicon Relat. Elem.* **1995**, *105*, 109−116.
(20) Jiang, G.; Gong, Z.; Li, X.-F.; Cullen, W. R.; Le, X. C. *Chem. Res. Toxicol.* **2003**, *16*, 873−880.
(21) Merrifield, M. E.; Ngu, T.; Stillman, M. J. *Biochem. Biophys. Res. Commun.* **2004**, *324*, 127−132.
(22) Toyama, M.; Yamashita, M.; Hirayama, N.; Murooka, Y. *J. Biochem. (Tokyo)* **2002**, *132*, 217−221.
(23) *Metallothionein*; Kagi, J. H. R., Nordberg, M., Eds.; Birkhauser: Boston, 1978; Vol. 1.
(24) *Metallothionein II*; Kagi, J. H. R., Kojima, Y., Eds.; Birkhauser: Boston, 1985; Vol. 2.
(25) *Metallothioneins*; Stillman, M. J., Shaw, C. F., III, Suzuki, K. T., Eds.; VCH Publishers: New York, 1992.
(26) *Metallothionein III*; Suzuki, K. T., Imura, N., Kimura, M., Eds.; Birkhauser: Boston, 1993; Vol. 3.
(27) Zelazowski, A. J.; Garvey, J. S.; Hoeschele, J. D. *Arch. Biochem. Biophys.* **1984**, *229*, 246−252.
(28) Garrett, S. H.; Belcastro, M.; Sens, M. A.; Somji, S.; Sens, D. A. *J. Toxicol. Environ. Health, Part A* **2001**, *64*, 343−355.
(29) Liu, J.; Liu, Y.; Goyer, R. A.; Achanzar, W.; Waalkes, M. P. *Toxicol. Sci.* **2000**, *55*, 460−467.
(30) Rigby, K. E.; Chan, J.; Mackie, J.; Stillman, M. J. *Proteins: Struct., Funct., Bioinf.* **2005**, *62*, 159−172.
(31) Gan, T.; Munoz, A.; Shaw, C. F., III; Petering, D. H. *J. Biol. Chem.* **1995**, *270*, 5339−5345.
(32) Zaia, J.; Fabris, D.; Wei, D.; Karpel, R. L.; Fenselau, C. *Protein Sci.* **1998**, *7*, 2398−2404.
(33) Li, H.; Otvos, J. D. *J. Inorg. Biochem.* **1998**, *70*, 187−194.
(34) Shaw, C. F., III; He, L.; Munoz, A.; Savas, M. M.; Chi, S.; Fink, C. L.; Gan, T.; Petering, D. H. *J. Biol. Inorg. Chem.* **1997**, *2*, 65−73.
(35) Munoz, A.; Petering, D. H.; Shaw, C. F., III. *Inorg. Chem.* **1999**, *38*, 5655−5659.
(36) Pattanaik, A.; Bachowski, G.; Laib, J.; Lemkuil, D.; Shaw, C. F., III; Petering, D. H.; Hitchcock, A.; Saryan, L. *J. Biol. Chem.* **1992**, *267*, 16121−16128.

flow UV−visible absorption and emission) could not provide the necessary detail. The exception to this is Zaia et al.[32] who used electrospray ionization mass spectrometry (ESI-MS) to identify the intermediates involved in metal transfer from MT to EDTA, carbonic anhydrase, a hexamer of insulin, and a DNA-binding protein and who first suggested that ESI-MS data could be used to generate a reaction time course for MT. Details of the metalation and metal transfer reactions of metallothionein are critically important to the overall description of the role of metallothionein as a metal chaperone.

We report here the complete temporal and transition state details of As^{3+} binding to the separate recombinant human (rh) α and β MT domains using specific time intervals and temperature-resolved ESI-MS. ESI-MS is a powerful tool with which to study kinetic reactions[32,39−41] because the reaction mixture can be injected directly into the spectrometer for online analysis, following reaction for specific times.[42] Further, and most importantly, ESI-MS allows for the identification and monitoring of intermediates on the basis of mass-to-charge ratios that cannot normally be identified and quantified using other techniques, especially at low concentrations.[32,39−41] Intensity−time profiles can be measured and rate constants obtained[42] following continuous flow mixing with direct infusion into the ESI-MS instrument. From these data, we describe the temperature-resolved metalation reactions of As-MT using ESI-MS to monitor each of the four species (metal-free, As_1-MT, As_2-MT, As_3-MT) throughout the reaction, allowing for the calculation of the kinetic and thermodynamic parameters of the transition state (rate constants, activation energies, activation enthalpies, and activation entropies) for the step-by-step metalation of the rh-α and rh-β MT domains with up to three As^{3+}. The experimentally determined parameters reported here allow for the simulation of the As^{3+} metalation reactions of MT with parameters set for any concentration or temperature in addition to those used in the experiment reported here.

Procedures

Materials and Methods. rh-MT was expressed in BL21(DE3) *Escherichia coli* cells that were transformed using a pP-1 plasmid that contains an S-tag as previously described.[43,44] The S-tag is used for stability during the purification process. The protein was further purified and demetalated by elution through a Sephadex G25 column using 25 mM ammonium formate at pH 2.7 (Fisher). Elution was monitored by UV−visible absorption at the characteristic MT wavelengths of 300−200 nm. Fractions that contained metal-free (apo) MT were collected, and purity was checked using ESI-MS. Previous reports have suggested or shown the existence of apo protein in vivo,[30,45−50] making the study of apo protein relevant as a starting point in exploring the metalation reactions of As^{3+}. The apo protein concentration was determined using the DTNB test (420 nm, 13 600 L mol^{-1} cm^{-1})[51,52] and from the extinction coefficient of 46 000 L mol^{-1} cm^{-1} at 220 nm. Protein concentrations ranged from 19 to 76 μM; however, for the kinetic ESI-MS experiments using the thermostatted mixing tee, only a 32 μM stock solution of apo αMT and a 19 μM stock solution of apo βMT were used. Oxidation is a significant problem with solutions of MT in these experiments. The apo protein was kept in its reduced state by carefully deoxygenating the sample by evacuating the sample and saturating with argon gas such that the protein was contained within a sealed inert environment. All protein samples were buffered in 25 mM ammonium formate at pH 2.7, which is ESI-MS friendly.

Solutions of 5 mM As^{3+} at pH 3.5 were prepared by dissolving As_2O_3 (AnalaR) with neat HCl (Caledon) and ultrapure deionized water (Barnstead). NH_4OH (7.4 M; Fisher) was used to raise the pH of the As^{3+} solutions. As^{3+} solutions were deoxygenated and contained within a sealed inert environment similarly to the apo protein samples. The recent report by Rey et al.[18] showed that $As(OH)_3$ is the major species between pH 1 and 7. Reactions were carried out at a pH range of 3 to 4 as this was the optimum range for product formation and stabilization and a pH that was also suggested to be used by Rey et al.[18] and Serves et al.[19] to stabilize As^{3+}. Immunostaining for MT has shown that MT is potentially located in acidic subcellular structures similar to lysosome in earthworms,[53] and MT is also located in the acidic lysosomes of kidneys,[54,55] making the study of As^{3+} binding at low pH of interest. A higher pH resulted in significant degradation of the protein products (data not shown), but the measured ESI-MS data did show that As^{3+} does still bind to form the As_3-MT domain. High salt concentrations could not be used in conjunction with the ESI-MS measurements. CD spectra of As_3-H_2-αMT showed no distinct absorption from 220 to 300 nm.

Caution: Arsenic is a highly toxic reagent; caution should be used when handling arsenic and its derivatives.

ESI-MS Procedures. All data were collected using a Micromass LCT mass spectrometer in the positive ion mode. The mass spectrometer was operated using the following parameters: 3551.0 V capillary, 42.0 V sample cone, 4.0 V extraction cone, acquisition scan time of 4 s, and interscan delay time of 0.4 s. The ESI-MS data were processed and deconvoluted using the Max Ent I software (Micromass).

Kinetic Measurements. Kinetic data were obtained using a thermostatted mixing "tee" attached directly to the input capillary of the ESI-MS instrument via a reaction capillary. The reaction mixing time is dependent on the length, diameter, and flow rate within the reaction capillary[41,42] and the short length of the input capillary. The exchangeable reaction capillary used had an inner diameter of 75 μm, with lengths ranging from 30 to 300 cm, and together with the input capillary gave reaction times of 102−1020 s and was contained within a temperature-controlled water bath. The input capillary did affect the average temperature of the reaction, particularly at the extreme low temperatures and short reaction times, leading to those data sets including slightly greater uncertainties, for example in Figure 9A,B, in which apo MT is at a lower relative abundance at 102 s than at 200 s. The temperature range used was 273−363 K. ESI-MS data were recorded for a wide range of stoichiometries by adjusting the individual flow rate of the pumps and hence the mixing ratio for the As^{3+} and

(37) Salgado, M. T.; Stillman, M. J. *Biochem. Biophys. Res. Commun.* **2004**, *318*, 73−80.
(38) Ejnik, J.; Robinson, J.; Zhu, J.; Forsterling, H.; Shaw, C. F., III; Petering, D. H. *J. Inorg. Biochem.* **2002**, *88*, 144−152.
(39) Bothner, B.; Chavez, R.; Wei, J.; Strupp, C.; Phung, Q.; Schneemann, A.; Siuzdak, G. *J. Biol. Chem.* **2000**, *275*, 13455−13459.
(40) Miranker, A.; Robinson, C. V.; Radford, S. E.; Dobson, C. M. *FASEB J.* **1996**, *10*, 93−101.
(41) Attwood, P. V.; Geeves, M. A. *Anal. Biochem.* **2004**, *334*, 382−389.
(42) Wilson, D. J.; Konermann, L. *Anal. Chem.* **2004**, *76*, 2537−2543.
(43) Merrifield, M. E.; Huang, Z.; Kille, P.; Stillman, M. J. *J. Inorg. Biochem.* **2002**, *88*, 153−172.
(44) Chan, J.; Huang, Z.; Merrifield, M. E.; Salgado, M. T.; Stillman, M. J. *Coord. Chem. Rev.* **2002**, *233−234*, 319−339.
(45) Pattanaik, A.; Shaw, C. F. I.; Petering, D. H.; Garvey, J. S.; Kraker, A. J. *J. Inorg. Biochem.* **1994**, *54*, 91−105.
(46) Rigby, K. E.; Stillman, M. J. *Biochem. Biophys. Res. Commun.* **2004**, *325*, 1271−1278.
(47) Hase, H.; Maret, W. *Anal. Biochem.* **2004**, *333*, 19−26.
(48) Yang, Y.; Maret, W.; Vallee, B. L. *Proc. Natl. Acad. Sci. U.S.A.* **2001**, *98*, 5556−5559.
(49) Shapiro, S. G.; Squibb, K. S.; Markowitz, L. A.; Cousins, R. J. *Biochem. J.* **1978**, *175*, 833−840.
(50) Krezoski, S. K.; Villalobos, J.; Shaw, C. F. I.; Petering, D. H. *Biochem. J.* **1998**, *255*, 483−491.
(51) Ellman, G. L. *Arch. Biochem. Biophys.* **1958**, *74*, 443−450.
(52) Ellman, G. L. *Arch. Biochem. Biophys.* **1959**, *82*, 70−77.
(53) Morgan, A. J.; Sturzenbaum, S. R.; Winters, C.; Grime, G. W.; Aziz, N. A. A.; Kille, P. *Ecotoxicol. Environ. Saf.* **2004**, *57*, 11−19.
(54) Klein, D.; Lichtmannegger, J.; Heinzmann, U.; Muller-Hocker, J.; Michaelsen, S.; Summer, K. H. *Eur. J. Clin. Invest.* **1998**, *28*, 302−310.
(55) Freedman, J. H.; Powers, L.; Peisach, J. *Biochemistry* **1986**, *25*, 2342−2349.

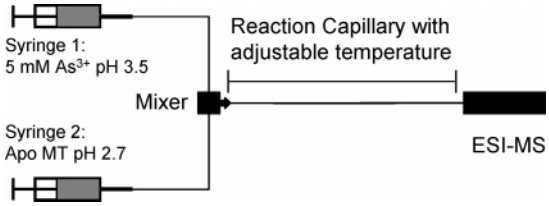

Figure 3. Schematic diagram of the continuous flow mixing set up for temperature-resolved ESI-MS measurements. Refer to the text for details.

Scheme 1 . Sequential Binding Mechanism Proposed for As^{3+} Binding to the α (A) and β (B) Domains of Human MT[a]

Scheme A – α MT

$$H_{11}\text{-}\alpha MT + As^{3+} \xrightarrow{k_{1\alpha}} As_1\text{-}H_8\text{-}\alpha MT$$
$$As_1\text{-}H_8\text{-}\alpha MT + As^{3+} \xrightarrow{k_{2\alpha}} As_2\text{-}H_5\text{-}\alpha MT$$
$$As_2\text{-}H_5\text{-}\alpha MT + As^{3+} \xrightarrow{k_{3\alpha}} As_3\text{-}H_2\text{-}\alpha MT$$

Scheme B – β MT

$$H_9\text{-}\beta MT + As^{3+} \xrightarrow{k_{1\beta}} As_1\text{-}H_6\text{-}\beta MT$$
$$As_1\text{-}H_6\text{-}\beta MT + As^{3+} \xrightarrow{k_{2\beta}} As_2\text{-}H_3\text{-}\beta MT$$
$$As_2\text{-}H_3\text{-}\beta MT + As^{3+} \xrightarrow{k_{3\beta}} As_3\text{-}\beta MT$$

[a] Rate constants for each step are indicated by $k_{1,2,3}$ (α or β), which are for the rate of adding a single As^{3+} to the metallothionein domain to form a product with n (1, 2, or 3) As^{3+} bound. This same nomenclature is used in Table 1 where the experimental values are reported.

protein solutions from 1:9 to 9:1 μL min^{-1} (total flow rate was always 10 μL min^{-1}) to give a sequence of mass transfer rates over a wide array of temperatures (273−363 K) for each of the reaction mixing times used (data not shown). Kinetic data were obtained by mixing the two streams of solutions as shown in Figure 3 with a flow rate of 2 μL/min for 5 mM As^{3+} solutions and 8 μL/min for protein solutions, for a total flow rate of 10 μL/min, which results in a final concentration after mixing of 26 μM for αMT, 16 μM for βMT, and 1 mM for As^{3+} and a ratio for As^{3+}:αMT and As^{3+}:βMT of 38.5:1 and 62.5:1, respectively. Note that, for the bimolecular reactions shown in Scheme 1 and the rate constants listed in Table 1, As^{3+}:αMT ratios of 1, 2, 3,8, 38, and 100 would give corresponding reaction completion times of approximately 2 h, 10 h, 70 h, 3.5 h, 20 min, and 10 min, respectively. It is clear that the greater the As^{3+} concentration the faster the reaction goes to completion, and for this experiment to be feasible, an excess of As^{3+} had to be used. Thus, the conditions used in these experiments were optimal for giving a reaction time resolution of seconds to minutes that allowed the reaction to be observed from the early stages all the way to completion for a wide range of temperatures. ESI-MS measurements were obtained using a wide scan range (100−2000 Da), and MS mass calculations were integrated from a minimum of 10 scans. The temperatures reported are an average with uncertainties of ±1 K of each other.

Supporting Information Figure S1 shows the linear relationship between reaction capillary length and the reaction time measured directly from the ESI-MS instrument by timing the appearance of the solution of a specific *m*/*z* species using each reaction capillary. Using NaI and CsI standards, we measured the time required to obtain a mass spectrum for each reaction length used in this study.

Data Analysis. We will briefly describe the rationale behind the data analysis used here. Further information can be found in the Supporting Information. Even when using large excesses of As^{3+}, it is clear that the data do not follow first-order kinetics (Figures 4 and 5, and data not shown from varying the flow rate as mentioned above). Three sequential second-order reactions (Scheme 1) are proposed to account for the observed kinetic data (Figures 4−6). The second-order mechanism proposed for each step of the sequential metalation (Scheme 1) fits the experimental data exceptionally well (vide infra), whereas a sequential first-order process did not fit the data (data not shown). The reactions shown in Figures 4, 5, S3, and S4 all proceed to completion with the formation of As_3-H_2-αMT or As_3-βMT with excess (>3 mol equiv) As^{3+} added. Under the nonequilibrium conditions of excess As^{3+} (38 and 62 times excess) and the short reaction times used for the kinetic measurements reported in Figures 6−8, the reverse reactions are not significant. Data analysis was carried out using the program Gepasi[56−58] with a second-order bimolecular irreversible mechanism model reaction.

For the kinetic analysis, we used the deconvoluted mass spectral data, which provided the relative abundances for all the MT species. Yu et al. have shown that the relative concentration of various Cd-MT species can be estimated from the relative abundances of the ions in the ESI spectrum.[59] The relative abundances of all the MT species observed in each mass spectrum were summed and normalized. The normalized relative abundances in each spectrum following a specific reaction mixing time were then plotted versus $1/T$ (K^{-1}), with T ranging from 273 to 363 K for each solution. As kinetic data are normally analyzed from concentration data as a function of time at a constant temperature, our kinetic data have been rearranged. This serves two purposes. First, the analysis follows traditional procedures. Second, the data may be directly compared to kinetic data obtained as a function of time at a fixed temperature. In addition, this serves to average many different independent data sets, improving confidence in the calculated results. The data sets were combined in terms of ln(Relative Abundance), and appropriate interpolation points were calculated for construction of 3D graphs with the axes ln(Relative Abundance), time (s), and $1/T$ (K^{-1}). These 3D plots are shown in Figure 6. From these 3D plots, slices were obtained of relative abundance as a function of time at fixed temperatures. These data sets were fitted according to Scheme 1 to determine the specific rate constants. The 3D plots shown in Figure 6 were constructed from a number of different solutions obtained over a series of days. Analysis of the residuals in the fitting (Figure S5) shows no bias and average to zero, providing evidence solely for the presence of random rather than systematic errors. Finally, the reliability of the method was confirmed by back-calculating the relative abundances of all species as a function of reaction time and temperature for comparison directly with the measured data (Figure 8).

Results

Figures S2−S4 show the steady-state ESI-MS spectra (including the charge states) measured for samples of metal-free, rh-apo α and β MT domains (Figure S2) and the two domains following complete saturation with As^{3+} (Figures S3 and S4). Metallothioneins generally exhibit an ESI mass spectrum with a series of charge states of measurable intensity between +4 and +10, depending on the metalation status and the pH of the measurement.[21,43,44,60,61] The charge states arise from protonation of basic amino acids present in the sequence. The ESI mass spectra of the apo α and β MT domains shown in Figure S2 (A and B) indicate the presence of a single species. The measured masses correlate well with the masses calculated from the sequence for α (6894.2 Da) and for β (6563.8 Da). Incubation of the two domains with excess As^{3+} at pH 3.5 results in formation of As_1-, As_2-, and As_3-containing domains. Analysis of the ESI-MS data shown in Figures S3 and S4 shows that a

(56) Mendes, P. *Comput. Appl. Biosci.* **1993**, *9*, 563−571.
(57) Mendes, P. *Trends Biochem. Sci.* **1997**, *22*, 361−363.
(58) Mendes, P.; Kell, D. B. *Bioinformatics* **1998**, *14*, 869−883.
(59) Yu, X.; Wojciechowski, M.; Fenselau, C. *Anal. Chem.* **1993**, *65*, 1355−1359.
(60) Merrifield, M. E.; Chaseley, J.; Kille, P.; Stillman, M. J. *Chem. Res. Toxicol.* **2006**, *19*, 365−375.
(61) Le Blanc, J. C. Y.; Presta, A.; Veinot, J.; Gibson, D.; Siu, K. W. M.; Stillman, M. J. *Protein Pept. Lett.* **1997**, *4*, 313−320.

Table 1. Rate Constants, Activation Energies (E_A), Arrhenius Factor (A), Activation Enthalpies ($\Delta H^{\ddagger}$), Activation Entropies ($\Delta S^{\ddagger}$), and Activation Free Energies ($\Delta G^{\ddagger}$) for the As^{3+}-Induced Metallation of the α- and the β MT Domains

arsenic species formed	n^a	$k_n{}^a$ at 298 K $M^{-1}\,s^{-1}$	E_A kJ mol^{-1}	A $\times 10^5\ s^{-1}$	$\Delta H^{\ddagger}$ kJ mol^{-1}	$\Delta S^{\ddagger}$ $JK^{-1}\,mol^{-1}$	$\Delta G^{\ddagger}$ at 298 K kJ mol^{-1}
As_1-H_6-β MT	1β	3.6	32	14.1	29	−135	69
As_2-H_3-β MT	2β	2.0	35	33.1	33	−128	71
As_3-β MT	3β	0.8	29	1.0	30	−146	73
As_1-H_8-αMT	1α	5.5	33	38.6	31	−127	69
As_2-H_5-αMT	2α	6.3	29	7.5	26	−141	68
As_3-H_2-αMT	3α	3.9	23	0.4	20	−165	69

[a] For reactions as shown in Scheme 1, where k_n refers to the rate constant for a single step that involves addition of a single As^{3+} forming a product with n As^{3+} bound.

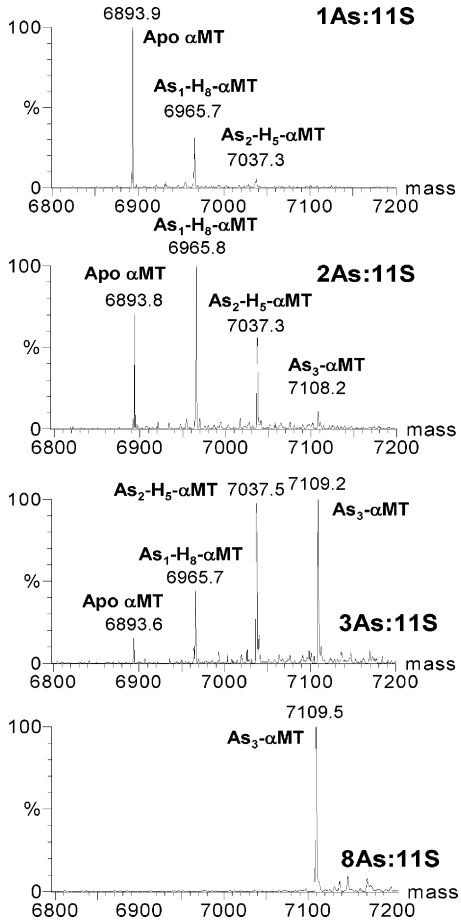

Figure 4. ESI mass spectrum of 36 μM apo αMT in the presence of increasing stoichiometric ratios (1, 2, 3, 8) of As^{3+}:αMT. Each sample was incubated for approximately 1 h at 296 K and pH 3.5 before measurement.

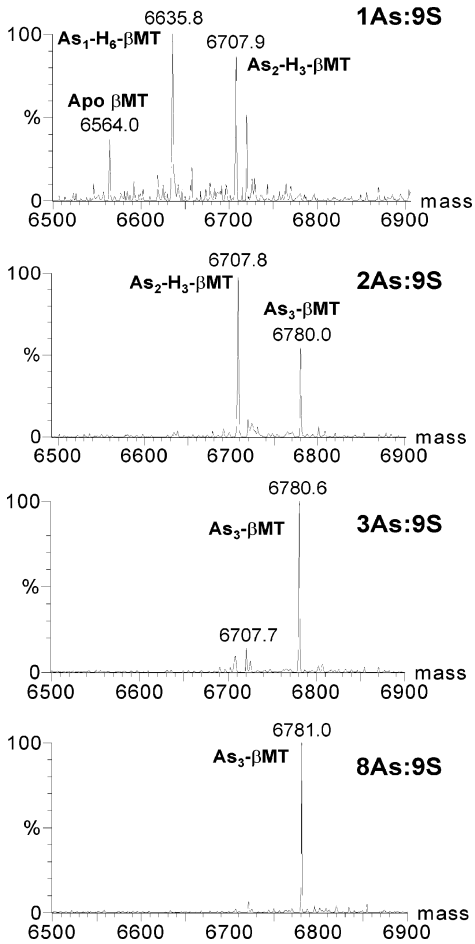

Figure 5. ESI mass spectrum of 76 μM apo β MT in the presence of increasing stoichiometric ratios of (1, 2, 3, 8) As^{3+}:β MT. All samples were incubated for approximately 1 h at 296 K and pH 3.5 before measurement.

maximum of three As^{3+} bind to each domain. Despite the domain stoichiometry of 4 for both Zn^{2+} and Cd^{2+} and 6[43,44] for Cu^{+} binding to αMT, there is no evidence of a fourth As^{3+} ion being bound to either the α or β domain. The estimated masses based on the metal content and amino acid sequence for H_{11}-αMT, As_1-H_8-αMT, As_2-H_5-αMT, and As_3-H_2-αMT are 6894.2, 6966.1, 7038.4, and 7109.9 Da, respectively, and the estimated mass based on the metal content and amino acid sequence for H_9-β MT, As_1-H_6-β MT, As_2-H_3-β MT, and As_3-β MT are 6564.7, 6636.6, 6708.5, and 6780.4 Da, respectively. The ESI-MS measured masses closely match the theoretical masses for these species.

Figures 4 and 5 show the As^{3+} concentration dependence on the metalated species formed for As^{3+} binding to each domain at 296 K following 1 h. As expected, a greater As^{3+} ratio results in an increase in the number of As^{3+} bound per MT domain within a set time. A stepwise increase in the As^{3+} concentrations for a series of MT solutions results in the final formation of As_3-H_2-αMT (Figure 4) and As_3-β MT (Figure 5) as the major products following incubation for an hour. Figures S3 and S4 show that As_3-β MT and As_3-H_2-αMT are also the predominant products of this reaction when excess As^{3+} is used. Figures S3 and S4 also show that the reaction time is dependent on the temperature, again as expected. From the relative abundances of the four protein species and the extent of the reaction measured following incubation for 1 h (Figures 4 and 5), we can determine that the reaction orders with respect to each of As^{3+} and MT are first order and second order for the overall reaction, which is confirmed by the application of the model

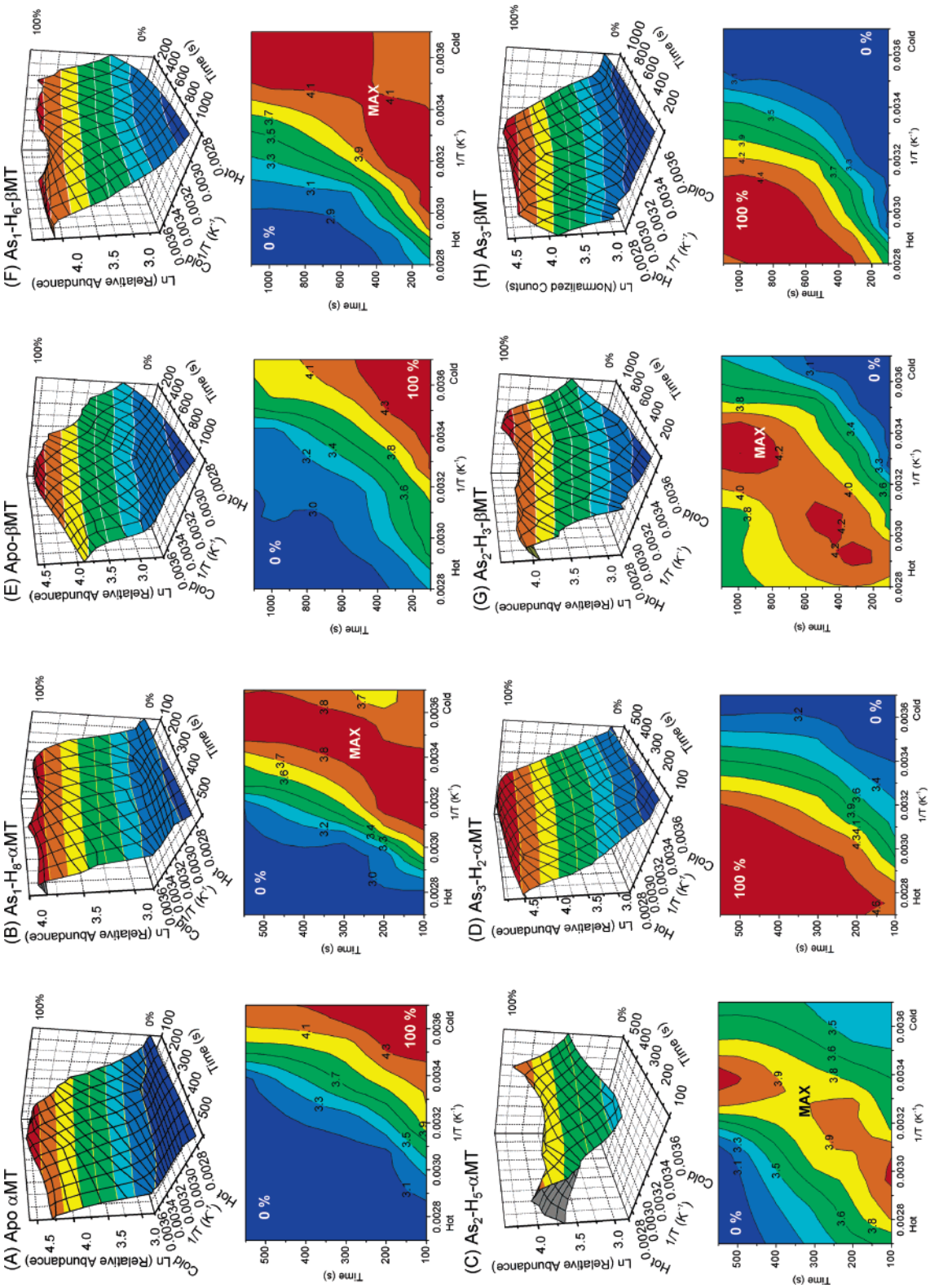

Figure 6. Trend in concentration of As_n-αMT ($n = 0-3$) (A−D) and As_n-βMT ($n = 0-3$) (E−H) as a function of temperature, $1/T$ (K^{-1}), and time (s) following mixing with the same molar ratio of As^{3+}. The diagrams were constructed from a series of ESI-MS traces recorded between 273 and 363 K and for reaction times between 102 and 1020 s, from different solutions each with an As^{3+}:MT stoichiometric ratio of 38.5:1 for the α domain and a ratio of 62.5:1 for the β domain. Solutions of 26 μM apo-αMT, 16 μM apo-βMT, and 1 mM As^{3+} solution were used after mixing. (Top) 3D visualization of ln(Relative Abundance) versus $1/T$, with reaction time (s) on the z-axis. (Bottom) Contour diagrams calculated from the 3D plot. It is important to note that to aid visualization of the trend in concentration as a function of time and temperature, each 3D plot has been orientated so that the 0% relative abundance is at the front. Hence, for the apo MT and As_1-MT, the conditions for 0% relative abundances are high temperatures and long reaction times because these two species are consumed as the reaction proceeds, whereas As_2-MT is both formed and consumed so that 0% abundance is found at both long and short times. We chose to display the short reaction times at cold temperatures. Low temperatures and short reaction times also favor 0% relative abundance of As_3-MT because it forms last. The contour diagrams provide more detail of the reaction profiles. Apo αMT (A), As_1-H_8-αMT (B), As_2-H_5-αMT (C), As_3-H_2-αMT (D), Apo βMT (E), As_1-H_6-βMT (F), As_2-H_3-βMT (G), and As_3-βMT (H).

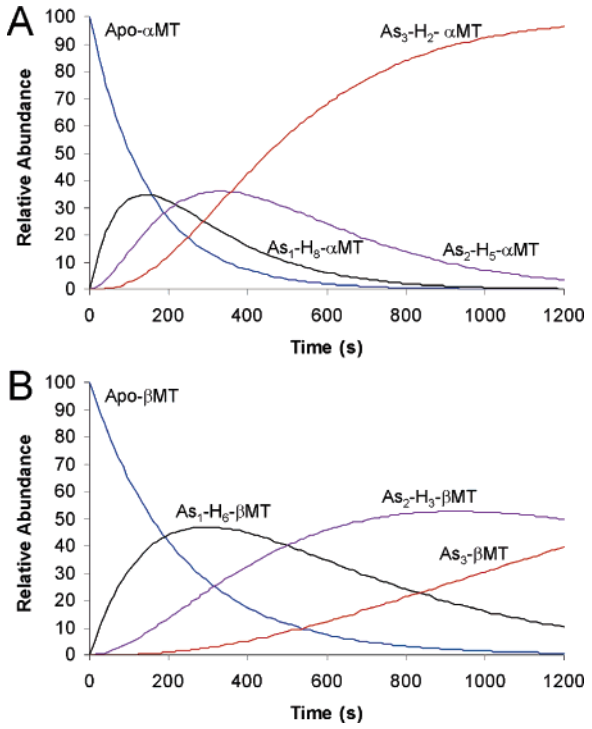

Figure 7. Simulation of the sequential binding mechanism shown in Scheme 1 for As^{3+} binding to the αMT (A) and βMT (B) domains over 1200 s. Time dependence of the fractional concentrations is plotted as the relative abundances of the four protein species that form following mixing of 26 μM apo α and 16 μM apo βMT domains with excess As^{3+} at 303 K using the derived parameters shown in Table 1. Modeled based on the As^{3+}:MT stoichiometric ratio of 38.5:1 for the α domain, a ratio of 62.5:1 for the β domain, and a 1 mM As^{3+} solution. The three specific rate constants for the reaction of As^{3+} with βMT are slower than that for the reaction of As^{3+} with αMT, resulting in the significantly slower formation of each species for βMT. The validity of the model can be confirmed by comparing the predicted relative abundances at selected times with the measured ESI-MS data under the same conditions. The model allows calculation of the reaction at temperatures between 273 and 363 K. Apo MT (blue), As_1-MT (black), As_2-MT (purple), and As_3-MT (red).

shown in Scheme 1. Even under pseudo-first-order conditions of excess As^{3+}, the reaction clearly follows a second-order mechanism (data not shown). The mass difference between peaks in the same charge state is approximately equivalent to the mass of 1 arsenic minus three protons, indicating that each As^{3+} ion binds three thiolates and displaces three protons. Figures S3 and S4 confirm that, with increased time and/or temperature, there is increased As^{3+} binding and with increased temperatures, faster binding. Within the range of the ESI-MS operating conditions, the thermostatted mixing tee was able to quantitatively measure the temperature and concentration dependence of the reaction of As^{3+} with the individual domains.

The kinetic data were then determined for a series of concentrations at fixed reaction times as a function of temperature. The data were rearranged into 3D representations showing the relative abundances of the apo, As_1-MT, As_2-MT, and As_3-MT as a function of both temperature and time (Figure 6). Interpolation in the ln(Relative Abundance) and $1/T$ (K^{-1}) directions allows for the assembly of trends in relative abundance as a function of both reaction time and temperature. Each set of data at a fixed temperature was analyzed using the sequential second-order reaction mechanism shown in Scheme 1. A plot of ln(k) versus $1/T$ (K^{-1}) was used to calculate the activation energies for each step in the sequential binding of

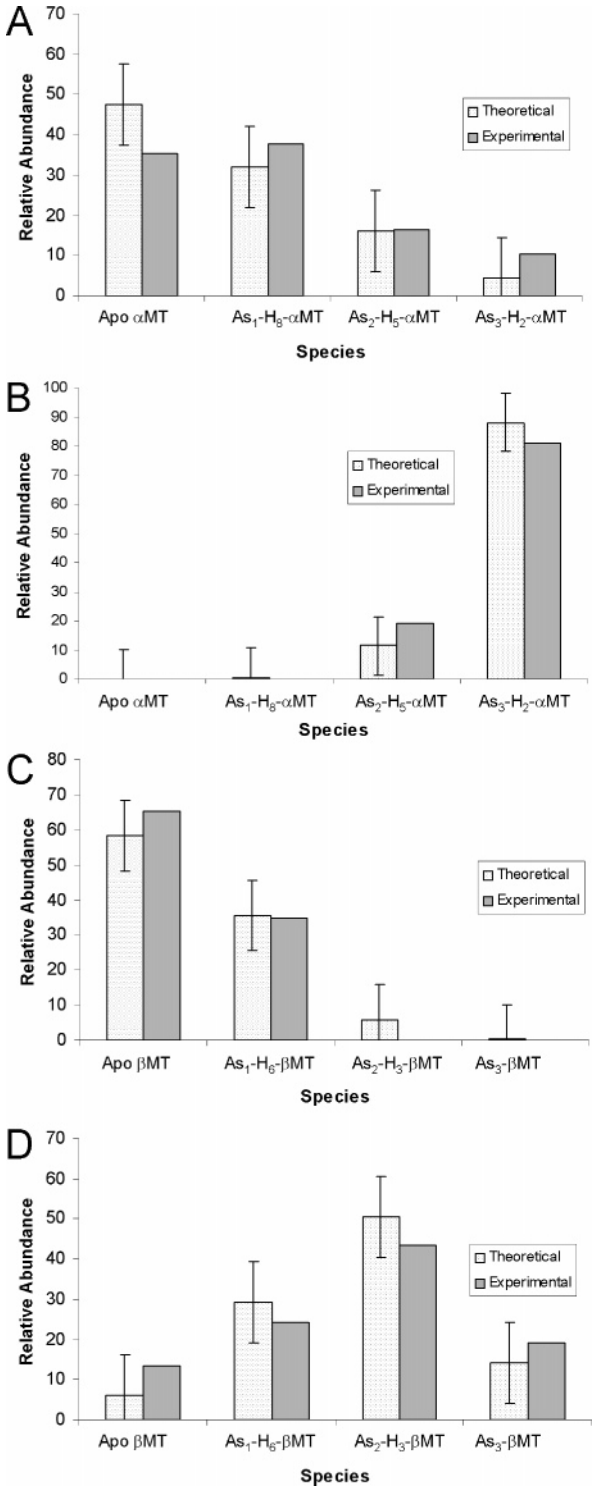

Figure 8. Comparison of experimental and theoretical relative abundances calculated for α (A, B) and β (C, D) MT domains at approximately 283 K (A, C) and 323 K (B, D) based on values from Table 1, a reaction time of 282 s, and using the model shown in Scheme 1. Conditions used were an As^{3+}:MT stoichiometric ratio of 38.5:1 for the α domain and a ratio of 62.5:1 for the β domain. Solutions of 26 μM apo αMT, 16 μM apo βMT, and 1 mM As^{3+} solution were used after mixing. The theoretical values from the simulation are within 10% of the experimental values.

As^{3+} to the separate domains (Figure S6). Kinetic and Erying transition state parameters obtained are given in Table 1.

It is a significant result of this study that we can report an accurate simulation of the relative concentrations of each of

the four components shown in Scheme 1 for the reactions between As^{3+} and the α and β domains as the reaction proceeds. The simulations (shown for a single temperature in Figure 7 for As^{3+} binding to αMT and βMT at 303 K) allow the concentrations of all four connected species (apo, As_1-MT, As_2-MT, and As_3-MT for either the α or the β domain) to be calculated as a function of reaction time for any temperature and concentration of the starting As^{3+} and protein. We carried out a major test of the accuracies of the simulations by calculating the relative abundances of each of the four component species for two specified temperatures (283 and 323 K) and for a specific reaction time (282 s) and comparing these data with the experimentally determined data sets. By selecting data sets at two temperatures in each of the reactions of α and β MT with As^{3+}, we test all the derived parameters listed in Table 1. Particularly, we calculated the temperature-dependent specific rate constants required for each simulation from the derived Arrhenius factors, $A_{1,2,3}$, and the activation energies, $E_{A1,2,3}$, which are based on the measured specific rate constants, $k_{1,2,3}$, for both the αMT and the βMT. The results of the comparison are shown in Figure 8.

Considering the kinetic data for the reaction of As^{3+} with αMT first (Figure 8A,B), we observe the expected trend: at 283 K the reaction is slow enough that the metal-free apo-MT still predominates, and only a small fraction of the final As_3-H_2-αMT is measured. Increasing the temperature results in a dramatic increase in the fractional composition of the As_3-H_2-αMT, as expected. The underlying trends are apparent from Figure 6 where the temperature and time dependence of the individual species are shown. Similarly close results are obtained when the simulation is carried out for the β domain (Figure 8C,D). The results for all four simulations are exceptionally good considering that the parameters were derived from about 30 different data sets per domain measured over a range of temperatures and times from a number of different experiments.

The data shown in Figure 8 provide important evidence that the simulations can be used to calculate the fractional compositions of such complicated reactions at temperatures and times not measured but within the range of the experimental data (Figure 6).

To further test the accuracy of the derived parameters shown in Table 1, we calculated the fractional compositions for As^{3+} reactions with each domain for all the data sets used to derive the underlying kinetic parameters reported in Table 1. This severely tests the reliability of both the measurement and the data analysis. Understandably, the errors will be larger because the experimental data themselves include errors of up to 20% on each relative abundance measurement depending on the temperature and reaction time. The predicted and experimental fractional compositions are shown in Figure 9. The agreement between the predicted relative abundances and the experimental data is exceptionally good, because the relative abundances in each experimentally determined mass spectrum are connected, so that errors in the relative abundance of one component will introduce compensating errors in the reported relative abundances of each of the other three components.

In Figure 9, we show the ESI-MS data obtained for each domain for a series of fixed reaction times at increasing temperatures. Shown are the results of eight simulations that predict the relative abundances as a function of temperature for mixing times of 102, 200, 282, 549, and 1020 s. In each of the panels, we plot the fractional composition of the solutions (apo MT and As_n-MT where $n = 1-3$) at fixed reaction times and for temperatures from 273 K to about 363 K. The measurements were carried out by varying the temperature for a set reaction time for solutions of the same concentration. The lines added represent a simulation of these data calculated following analysis to extract the specific rate constants at each temperature, A, and E_A for each of the three steps in the sequential bimolecular reaction (Scheme 1) using all data shown in the analysis. Taking these parameters, the fractional composition can be predicted for all conditions of concentration, temperature, and reaction time.

Considering the data and simulation shown in Figure 9A for As^{3+} mixed with αMT, we see how the relative abundances of As_1-αMT and As_2-αMT increase and then decrease as the temperature increases, whereas the relative abundance of apo MT decreases to zero at 360 K, and the relative abundance of As_3-αMT increases toward 370 K. These data represent the complete set of kinetic products following reaction for a set time. Increasing the reaction time to 200 s (Figure 9B), 282 s (Figure 9C), and 549 s (Figure 9D) results in formation of each As_n-MT species ($n = 1-3$) at successively lower temperatures as expected. Figure 9E−H shows the results of a similar series of experiments for As^{3+} reacting with apo βMT. Note, however, that the reaction between As^{3+} and the β domain requires nearly twice the time to reach completion as the reaction between As^{3+} and the α domain.

As described earlier, the lines in Figure 9 are connecting points that are based on the calculated kinetic parameters shown in Table 1. These smooth lines were calculated from the E_A's determined from the plot of ln(k) versus $1/T$ (K^{-1}) for each temperature observed. The theoretical lines, which can only be calculated when the entire data set of many different experiments is analyzed, are remarkably good when compared to the original data considering the inherent uncertainties (up to 20%) when many experimental data sets are combined. The error in these parameters is potentially compounded at every step of the analysis. We believe that these theoretical estimates provide an important and convincing validation of the technique we have used and show how temporal and temperature-resolved MS data could be used to obtain detailed kinetic parameters for complex multistep systems.

Discussion

The ubiquitous nature of MT underlies its importance in the cell and its connection with the cellular chemistry of metal transport and metabolism. The study of arsenic reactions in the mammalian system is important to our understanding of arsenic's metabolic pathway. Greater detail is needed about which proteins react with arsenic, the oxidation state of the arsenic, the rate constants from the reaction, the mechanism of the reaction, and the coordination environment in the chelating ligand or protein. The details of the reaction of MT with arsenic may help to answer some of these questions and may serve as a model for how arsenic interacts with other thiol-containing proteins.[20] For example, consider the reduction of As^{5+} to As^{3+} by arsenic reductases.[11] MT has also been shown to reduce metals, Cr^{6+} to Cr^{5+},[62] As^{5+} to As^{3+},[20] and Cu^{2+} to Cu^{+}.[37]

The ESI-MS experiments allowed for the direct determination of the time dependence of the fractional composition of each

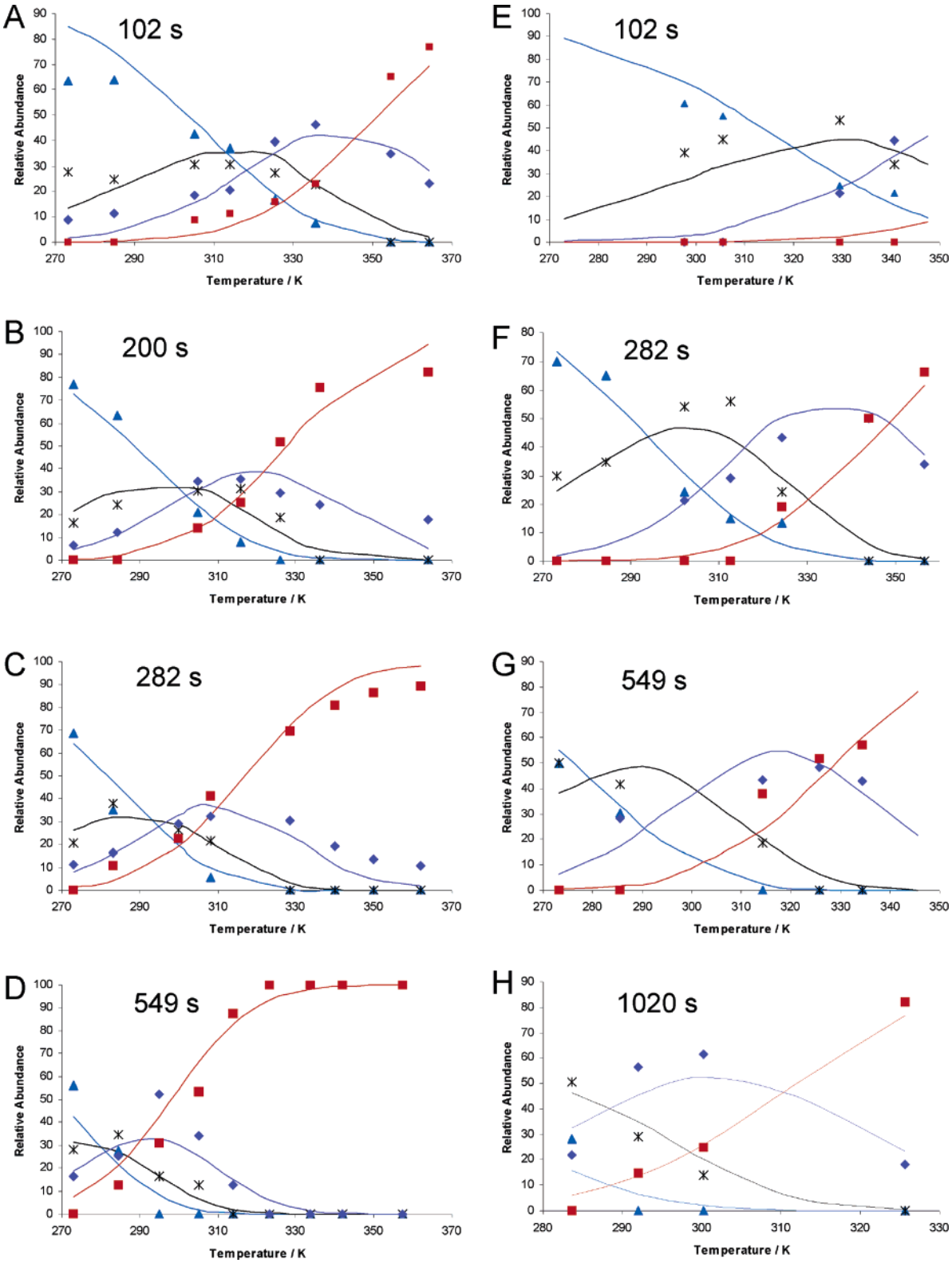

Figure 9. Temperature-resolved relative abundances for apo MT and As_n-MT ($n = 1-3$) following reaction with As^{3+} at fixed reaction times. Kinetic ESI-MS data obtained for apo αMT (A−D) and apo βMT (E−H) for a series of fixed reaction times at increasing temperatures (272−363 K) in the presence of excess As^{3+}. Fixed reaction times were 102 s (A, E), 200 s (B), 282 s (C, F), 549 s (D, G), and 1020 s (H). Reaction was carried out on As^{3+}:MT stoichiometric ratio of 38.5:1 for the α domain and a ratio of 62.5:1 for the β domain. Solutions of 26 μM apo αMT, 16 μM apo βMT, and 1 mM As^{3+} solution were used after mixing. The species for both the α and β domains are as follows: apo MT (blue ▲), As_1-MT (black *), As_2-MT (purple ◆), and As_3-MT (red ■). The smooth lines are calculated on the basis of the complete analysis of the kinetic data for the relative abundance at each temperature at the specified times. The lines are connected by the series of three sequential reactions shown in Scheme 1 and described in the text. The data points that comprise the theoretical lines were calculated from analysis of data sets measured at all reaction times and temperatures to obtain the kinetic parameters k_{temp}, A, and E_a, which were used with the experimental concentrations of the protein and the As^{3+} to predict the concentration of each species at the specified temperature and time. There will be considerable uncertainty in the simulation that uses parameters extracted from the entire temperature−time−relative abundance data set that comprises many different experiments.

key species as a function of temperature following the addition of As^{3+} to the α and β domains of MT. From these data, we have constructed the first model. We report the successive rate constants for the reaction of up to three As^{3+} with the isolated α and β metallothionein domains. Uncommonly for metalation reactions of MT, it was possible under these experimental conditions to obtain data that provide simultaneous estimates of the concentrations of all four species throughout the entire reaction. The relative abundances of each species are linked by the specific rate constants, k_n ($n = 1-3$) and E_A ($n = 1-3$), such that within the time required to reach equilibrium, the As^{3+}: MT distribution changes. Thus, each step in the As^{3+} metalation of the α or β MT domain follows a second-order process that has the following rate law: rate $= k_n[As_{n-1}MT][As^{3+}]$.

The relative abundances of all species as a function of temperature (Figures 6, 8, and 9) provide convincing evidence that the reaction is sequential and does not involve cooperative binding. The model shown in Scheme 1 and Figure 7 further confirms this.

Previous studies have indicated that one As^{3+} preferentially binds three thiols.[19] For the β domain, which contains nine cysteines, three As^{3+} are bound leaving no cysteines protonated and nine protons displaced. However, for the α domain, there are 11 cysteines, and with only three As^{3+} bound, two cysteines are protonated and nine protons are displaced. Interestingly, no fourth As^{3+} was ever observed bound. In particular, As_3-H_2-αMT, which had two free cysteines, was not observed to bind a fourth As^{3+}. The two domains, therefore, bind a total of six As^{3+}, which correlates to the maximum number of As^{3+} bound by mammalian holo-MT reported by Jiang et al.[20]

Our data show that the α domain binds As^{3+} nearly twice as fast as the β domain. This is consistent with previous studies showing that the α domain reacts faster than the β domain with aurothiomalate.[35] The difference in the reaction rates for each domain may be better understood by considering the lower thermodynamic stability of the β domain relative to that of the α domain.[33,63] The lowered stability of the β domain could affect the ability of the domain to bind As^{3+}, resulting in a slower binding rate.

Mechanism of Binding and Coordination for As^{3+}. Scheme 1 shows a mechanism in which sequential binding of As^{3+} takes place and which correlated well to the experimental data as a function of time and temperature. The MS data presented in Figures 6, 8, and 9 show that the final product is the As_3 α or β MT domain and that the mono- and di-As^{3+} loaded species were intermediates during the reaction. This then indicates that As^{3+} binding occurs sequentially rather then cooperatively. Cooperative binding would appear to be the mechanism if the predominate species present had been apo MT and As_3-MT. We propose that the As^{3+} does not bind in a clustered binding site as observed with other metals (e.g., Cd^{2+}),[44,64] as only three As^{3+} ions bind in the α domain and there is no evidence of thiolate bridging, which is characteristic of cluster formation in MT. If bridging were occurring, then we believe that a fourth As^{3+} ion would have been observed bound in the α domain. On the basis of the inorganic chemistry of As^{3+}, we speculate that each As^{3+} bound to three sulfurs has trigonal pyramidal coordination with the sulfurs acting as terminal ligands. Trialkyl trithioarsenite, $As(SR)_3$, compounds have been reported with trigonal-pyramidal coordination geometry.[65,66]

Implications of the Values of the Kinetic and Erying Transition State Parameters. Petering and co-workers have reported zinc, cadmium, cobalt,[38] and chromium[62] metalation reactions of metallothionein using stopped-flow techniques. The kinetics of Cd^{2+} and Zn^{2+} metalation have been reported to be mostly complete within the 4-ms dead time by stopped-flow UV−visible spectroscopy at pH 7 and room temperature.[38] Thus, the As^{3+} metalation reaction is much slower than the Cd^{2+} or Zn^{2+} metalation reaction

Table 1 lists the values of the rate constants for the single steps shown in Scheme 1 involving addition of a single As^{3+}. Within experimental error, the k_n decreases for each addition of As^{3+}, indicating the noncooperative nature of As^{3+} binding. The rate of As^{3+} binding is approximately two times slower for the β domain compared with the α domain. In addition, and as is clear from Figure 7, the relatively slower third step in the β domain results in a buildup in As_1-H_6-βMT species, which becomes the dominant species in the early part of the reaction with nearly 50% of the metallothionein formed with a single As^{3+}, whereas in the α domain As_3-H_2-αMT forms fast enough to ensure no buildup of the intermediates and dominates the speciation after 400 s. These observations can be seen quantitatively in the ratios of the rate constant for each step and each domain: $k_{1\alpha}:k_{1\beta} = 1.5$, $k_{2\alpha}:k_{2\beta} = 3.1$, and $k_{3\alpha}:k_{3\beta} = 4.9$, showing how much faster the metalation of the α domain is. The origins of these differences may be the presence of the extra cysteines in the α domain. The greater chain length may also reduce potential strain in the metal binding reaction, increasing the rates.

The activation energies for the reactions of each species are listed in Table 1. For the α domain, E_A decreases from 33 kJ mol^{-1} for As_1-H_8-αMT to 23 kJ mol^{-1} for As_3-H_2-αMT. The β domain differs in that E_A is approximately equivalent for all the species formed when considering the errors. The α domain has a lower activation energy than the β domain, and this may be the result of having two additional cysteines compared to the β domain. We can use the value of the Arrhenius constant (A) from Table 1 to obtain an indication of the change in collision frequency, even though A is more appropriate for gas-phase reactions. The A values from Table 1 show that, for both the α and β domains, there is a decrease in the number of collisions with the correct orientation to form the product between the first and third metal bound. We can speculate that, when the first As^{3+} binds, it is statistically favored as there are many thiolates available, but upon binding a third As^{3+} this becomes increasingly unlikely. Increasing the As^{3+} concentration would favor an increased chance of a correct collision, which correlates with the observed dependence of the rate on As^{3+} concentration. The slow step in this reaction must involve the binding of As^{3+} to MT, as the experimental data show a second-order mechanism that is As^{3+} and MT concentration-dependent. If we consider that the peptide backbone would have to wrap in such a manner that three thiolates are in close

(62) Krepkiy, D.; Antholine, W. E.; Petering, D. H. *Chem. Res. Toxicol.* **2003**, *16*, 750−756.
(63) Dalgarno, D. C.; Armitage, I. M. In *Advances in Inorganic Biochemistry*; Marzilli, L. G., Ed.; Elsevier: New York, 1984; Vol. 6, pp 133−138.
(64) Chan, J.; Merrifield, M. E.; Soldatov, A. V.; Stillman, M. J. *Inorg. Chem.* **2005**, *44*, 4923−4933.
(65) Chou, J.-H.; Kanatzidis, M. G. *Inorg. Chem.* **1993**, *33*, 5372−5373.
(66) Farrer, B. T.; McClure, C. P.; Penner-Hahn, J. E.; Pecoraro, V. L. *Inorg. Chem.* **2000**, *39*, 5422−5423.

proximity to bind the third As^{3+} ion, than the lower E_A may be due to the protein being rearranged into a position that allows the thiolates to bind the third As^{3+} easily. The binding of the As^{3+} is not expected to be the slow step, as the binding of thiolates to As^{3+} has previously been reported as fast.[67] In fact, the binding of the second and third thiolates to As^{3+} is orders of magnitudes faster than that of the first thiolates.[67] This suggests that the wrapping of the peptide or the rearrangement of the peptide to bring the cysteines close enough to bind the As^{3+} ion may be one of the slow steps. Further, we speculate that the slow step may in fact be the formation of the AsS_{cys3}, which implies that AsS_{cys1} and AsS_{cys2} dissociate rapidly and are not observed. In Figure S6, we observe that the plot of ln-(k_n) versus $1/T$ for the third step is quite nonlinear. Although we have estimated E_A from the slope of all the points plotted, it is possible that two mechanisms are operating over the temperature range used. The addition of the third and final As^{3+} to the binding site in each domain may well be more complicated than for the first two metals, and this might be observed as nonlinear behavior in the rate constant properties. However, further mechanistic details will require new experimental data.

Metalation Reactions of Metalloproteins. Few studies of the time-resolved metalation/folding of metalloproteins or even smaller peptides have been reported[68] in which the concentrations of each of the component species are measurable throughout the reaction; this is especially true of metalloproteins in which more than one metal bind, such as the iron−sulfur proteins, and the metallothioneins. An obvious problem is the lack of distinct spectroscopic probes that can be used to detect complex formation at low concentrations. The ESI-MS data reported here provide a new view of a complete metalation reaction.[32] Measurements as early as 100 ms after mixing are possible,[69] and the temperature resolution described here allows the reaction to be slowed or sped up over a considerable range, especially when concentration is factored in using the flow rate of the pumps.

Progress toward the Determination of Protein Molecular Structure in Solutions. The ESI-MS experiment has provided information previously unobtainable since all intermediates are visible in the mass spectrum and generally are not masked by similar molecular domains. Structural information about proteins has previously been determined from hydrogen−deuterium exchange[70] and protein folding through the presence of multiple charge states series that arise from the differing numbers of exposed basic residues for different conformations.[42,71,72] These techniques increase our understanding of the dynamic processes taking place as the measurements can be acquired rapidly and in real time following chemically induced changes. We report here that similar important information about binding reactions (and the reactions can be of any type, not just metalation, although metalation is our focus) can be obtained through temperature changes. The ESI-MS experiment is fast enough to allow the full range of temperature-dependent kinetic studies to be carried out and provides details about changes in relative abundances on a time scale of milliseconds.[69]

Developments in Quantifying the Metalation Reactions of Metallothionein. To the best of our knowledge, very few articles report on the kinetics of the metalation reactions of metallothionein.[32,37,38,62,73,74] We show for the first time the sequential rate constants for each step of the complete metalation of the isolated apo α and β domains. It should noted though that the holo MT protein may not necessary be the sum of a simple set of rate constants shown here. These data for arsenic binding allow for the mechanism to be determined unambiguously as sequential rather than cooperative because the relative abundances of the four key components have been measured at each time step. Finally, although As^{3+} has previously been reported to bind to metallothioneins,[20−22] we now show the stoichiometric ratios per domain and that, unusual for metallothionein, As^{3+} binding does not involve clusters; rather, the data suggest a series of three AsS_3 groups in which the nonbonding pair on the As^{3+} ion is presumably blocking the fourth cysteine and the three other valence electrons from As^{3+} are forming bonds with the sulfurs from cysteines.[75] We anticipate that analysis of the metalation reactions involving a range of metals can now be carried out using these new techniques and the complete metalation chemistry can be finally determined.

Conclusions

The results presented here provide the complete kinetic analysis and subsequent mechanism for the metalation of the α and β metallothionein domains and illustrate the use of online mixing and temperature-resolved ESI-MS as powerful tools in bioinorganic chemistry. The metalation of MT is described by three sequential bimolecular reactions occurring in a stepwise fashion suggesting a noncooperative binding mechanism. The rate of binding the second and third As^{3+} ions is limited by arrangement of the peptide backbone and the orientation of the As^{3+} rather then the formation of the $As-S_{cys}$ bond.

Acknowledgment. We thank NSERC of Canada for financial support through operating funds (to M.J.S.), Undergraduate Summer Research Award (USRA), and Ontario Graduate Scholarship (OGS) (to T.T.N.). We thank Prof. R. J. Puddephatt for use of the ESI-MS funded by the Canada Research Chair program. We are grateful to Doug Harsine for advice and discussion on the operation of the ESI-MS. We thank the reviewers for insightful comments.

Supporting Information Available: Six figures (S1−S6) and one scheme, together with descriptive text, showing steady-state ESI mass spectral data referred to in the text. This material is available free of charge via the Internet at http://pubs.acs.org.

JA062914C

(67) Spuches, A. M.; Kruszyna, H. G.; Rich, A. M.; Wilcox, D. E. *Inorg. Chem.* **2005**, *44*, 2964−2972.
(68) Ghosh, D.; Pecoraro, V. L. *Inorg. Chem.* **2004**, *43*, 7902−7915.
(69) Zechel, D. L.; Konermann, L.; Withers, S. G.; Douglas, D. J. *Biochemistry* **1998**, *37*, 7664−7669.
(70) Yan, X.; Watson, J.; Ho, P. S.; Deinzer, M. L. *Mol. Cell. Proteomics* **2004**, *3*, 10−23.
(71) Pan, H.; Raza, A. S.; Smith, D. L. *J. Mol. Biol.* **2004**, *336*, 1251−1263.
(72) Cunsolo, V.; Foti, S.; Rosa, C. L.; Saletti, R.; Canters, G. W.; Verbeet, M. P. *J. Mass Spectrom.* **2003**, *38*, 502−509.
(73) Palumaa, P.; Eriste, K.; Kruusel, K.; Kangur, L.; Joernvall, H.; Sillard, R. *Cell. Mol. Biol.* **2003**, *49*, 763−768.
(74) Hathout, Y.; Fabris, D.; Fenselau, C. *Int. J. Mass Spectrom.* **2001**, *204*, 1−6.
(75) Housecroft, C. E.; Sharpe, A. G. *Inorganic Chemistry*, 2nd ed.; Pearson Prentice Hall: Harlow, England, 2005.